Hagedorn et al., http://www.jcb.org/cgi/content/full/jcb.201301091/DC1

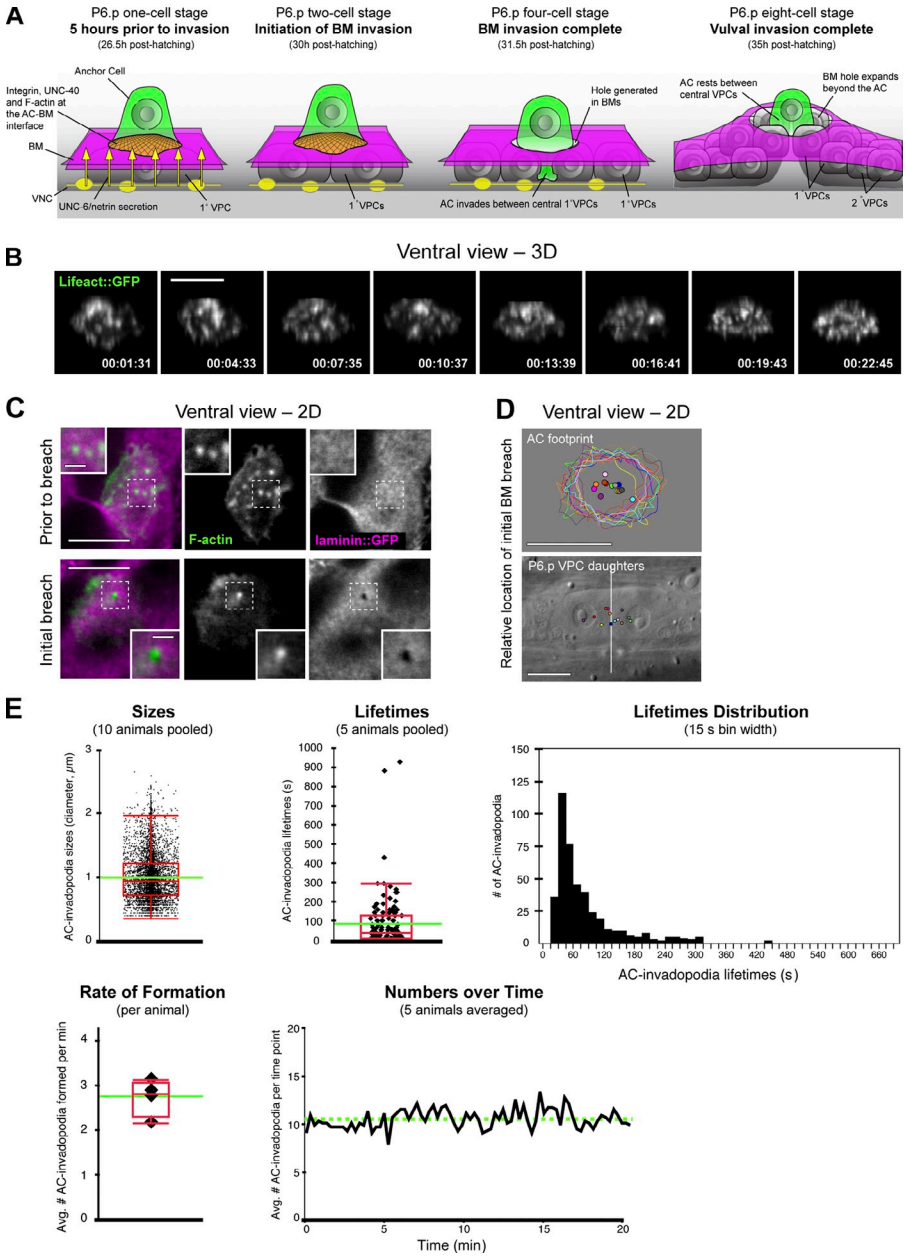

Figure S1. **AC-invadopodia breach the basement membrane.** (A) Schematic diagram depicts four developmental time points over the course of AC invasion in *C. elegans* (times shown are after hatching at 20°C). 5 h before invasion, at the P6.p one-cell stage, the integrin receptor INA-1/PAT-3 and the netrin receptor UNC-40 (DCC) localize to the invasive cell membrane and regulate a polarized F-actin–rich membrane domain (orange) within the AC (green) at the basement membrane (BM) interface (magenta). AC invasion initiates at the P6.p two-cell stage and by the P6.p four-cell stage the AC clears a large gap in the basement membrane and moves between the central P6.p vulval cells. By the P6.p eight-cell stage, the invaginating vulval cells have expanded the gap in the basement membrane beyond the AC, where it then stabilizes in its position. At this time the AC is situated at the apex of the vulva between the central vulval cells. (B) A ventral view time series of an AC-specific Lifeact::GFP probe (*cdh-3 > Lifeact::GFP*), an alternative F-actin marker, reveals dynamic F-actin–rich invadopodia along the invasive cell membrane of the AC. Images were acquired using a lateral view of the animal and then rotated on the z axis, resulting in some cropping of the most proximal part of the image (top of images shown). Bar, 5 µm. (C) Ventral view images show F-actin–rich AC-invadopodia (middle, expressing *cdh-3 >* mCherry::moeABD) in relation to the basement membrane (left, overlay; right, viewed with laminin::GFP). AC-invadopodia form before breach (top, dashed boxes, insets) and occupy the initial breach site (bottom, dashed boxes, insets). Bars: (main images) 5 µm; (insets) 1 µm. (D) The diagrams depict the location of the initial basement membrane breach (spots) relative to the footprint of the AC (top, outlines) and underlying P6.p vulval cells (bottom, vertical white line marks the interface of the central vulval cells; *n* = 13 animals). Each color represents the same animal. (E) The graphs show quantitative data of wild-type AC-invadopodia in the hour preceding basement membrane invasion. Green lines denote population means for measurements of size (1.00 µm; *n* = 8,182 structures), lifetime (1.13 min; *n* = 729 structures), rate of formation (2.8 structures per minute), and numbers over time (11 structures); red boxes show the interquartile range and whiskers show 1.5 × interquartile range. The same data are shown in the lifetimes and lifetimes distribution graph.

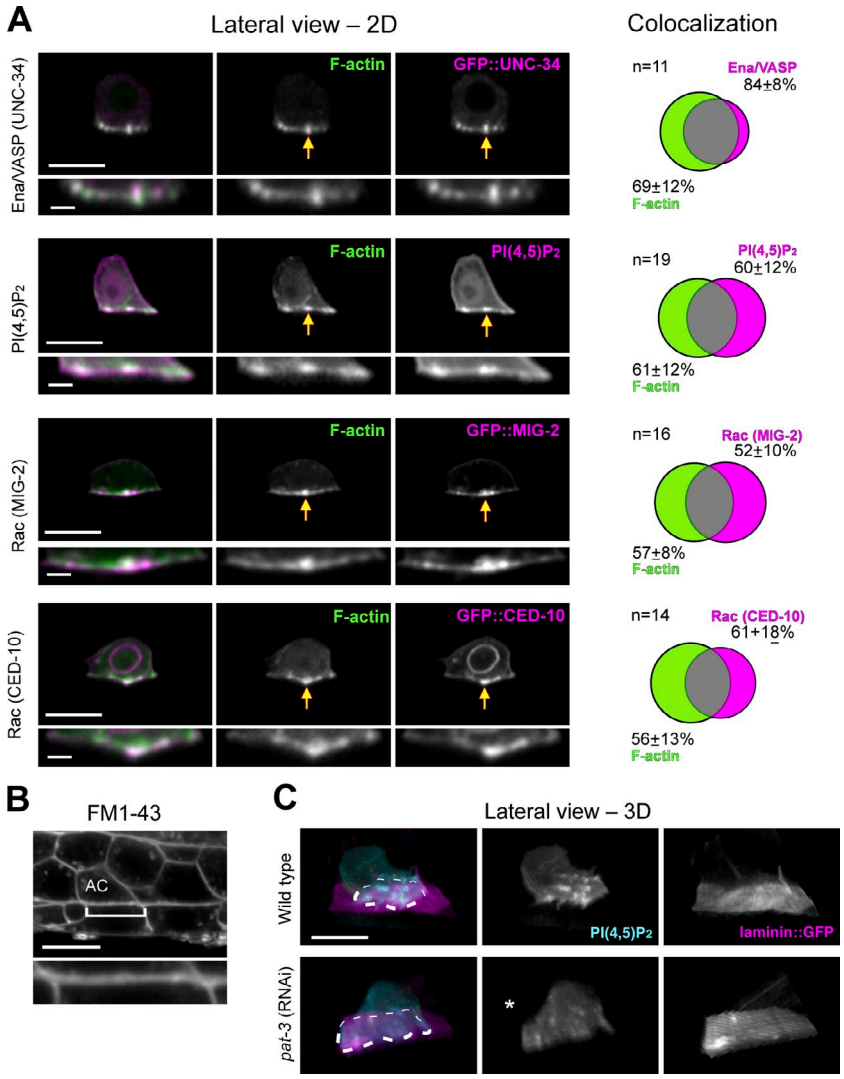

Figure S2. **AC-invadopodia are enriched in actin regulators and are dependent on integrin.** (A) Lateral view images show ACs coexpressing the F-actin marker *cdh-3* > mCherry::moeABD (green in overlays) and one of four GFP-tagged proteins (GFP::UNC-34, mCherry::PLCδ^{PH} [PI(4,5)P_2], GFP::MIG-2, and GFP::CED-10; magenta in overlays). Arrows point to colocalization at F-actin structures; insets show magnification of the invasive cell membrane. Venn diagrams (right) display the percentage of total volume colocalized for each protein. The mean percent overlap ± SD is reported. Bars: (main images) 5 µm; (insets) 1 µm. (B) The vital dye FM1-43, which labels the outer leaflet of the plasma membrane, was not enriched at invadopodia structures at the AC–basement membrane interface (bracket). (C) Images show 3D reconstructions of confocal z-stacks rotated forward. The AC is expressing the PI(4,5)P_2 marker *cdh-3* > mCherry::PLCδ^{PH} (cyan). The basement membrane is visualized with laminin::GFP (magenta). In wild-type animals (top) many invadopodia are present along the invasive cell membrane of the AC (outlined with a dashed circle in the overlay). RNAi knockdown of *pat-3* (bottom), the β-subunit of the integrin heterodimer INA-1/PAT-3, resulted in a dramatic reduction in invadopodia formation (asterisk; similar results observed in eight animals).

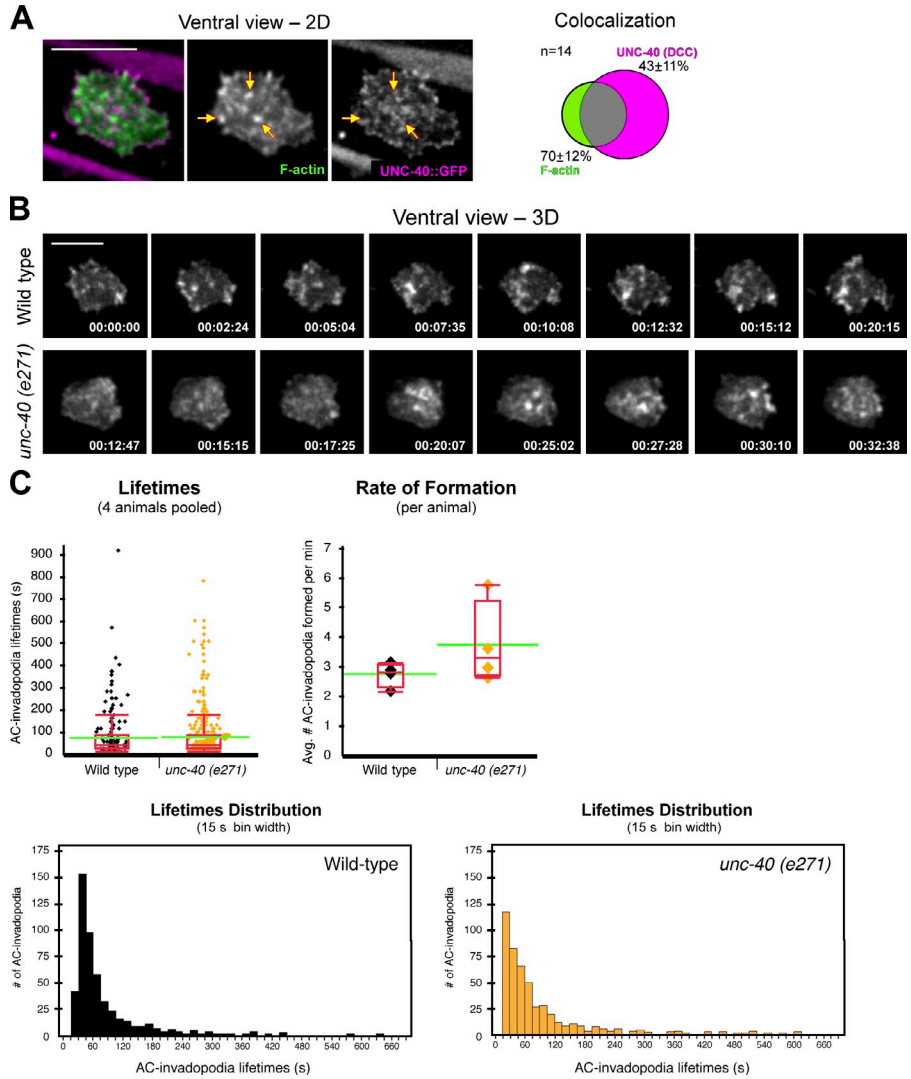

Figure S3. **UNC-40 does not localize to invadopodia or regulate their dynamics.** (A) Lateral view images show an AC coexpressing the F-actin marker *cdh-3* > mCherry::moeABD (green in overlay) and UNC-40::GFP (magenta). Arrows highlight F-actin–rich AC-invadopodia that lack specific enrichment of UNC-40::GFP. Venn diagram (right) shows the percentage of total volume colocalized for UNC-40 and F-actin. The mean percent overlap ± SD is reported. (B) Ventral view time series show similar invadopodia dynamics (viewed with *cdh-3* > mCherry::moeABD) in wild type (top) and *unc-40* mutants (bottom). Bars, 5 µm. (C) Graphs show quantitative analysis of invadopodia lifetimes and rate of formation in wild-type animals and in *unc-40 (e271)* mutants. Red boxes mark the interquartile range and whiskers show 1.5 × interquartile range. Green lines denote population means for measurements. Wild-type invadopodia had mean lifetimes of 84 s and formed at a mean rate of 2.8 structures per minute (n = 309 structures from four animals). In *unc-40* mutants, invadopodia had mean lifetimes of 81 s and formed at a mean rate of 3.8 structures per minute (n = 473 structures from four animals). No statistical differences were observed ($P > 0.05$, Wilcoxon rank-sum test). The same data for wild type and *unc-40 (e271)* is reported in the lifetimes graph (top left) and lifetimes distribution graphs (bottom). The error bars represent the SEM.

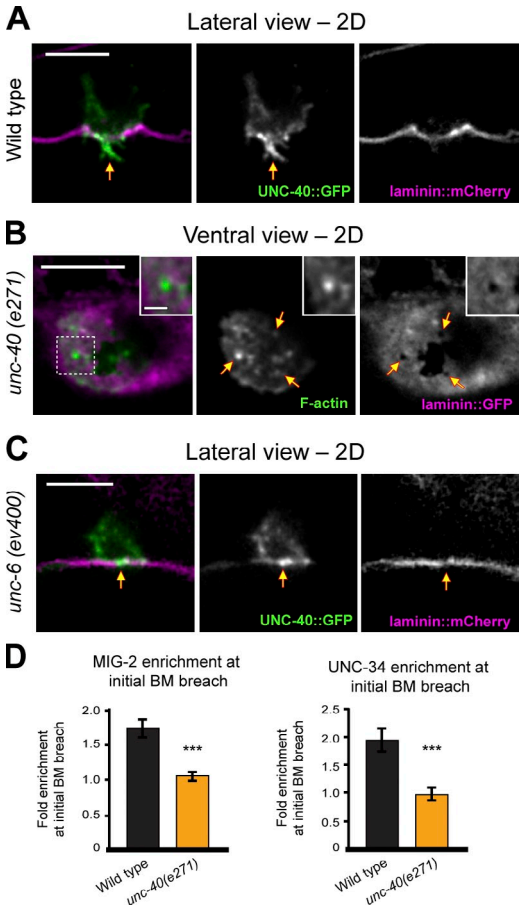

Figure S4. **UNC-40 localization and regulation of invadopodia breaching.** (A) Lateral view images show an AC coexpressing UNC-40::GFP (green in overlay) and laminin::mCherry (labeling the basement membrane; magenta). Arrows highlight UNC-40::GFP enriched in the invasive protrusion. (B) Ventral view images show AC-invadopodia (viewed with *cdh-3* > mCherry::moeABD; green) and the basement membrane component laminin::GFP (magenta) in an *unc-40* mutant animal. Invadopodia occupy multiple breaches in the basement membrane (arrows; dashed box corresponds to inset). Bars: (main images) 5 µm; (insets) 1 µm. (C) Lateral view images show an AC coexpressing UNC-40::GFP (green in overlay) and the basement membrane component laminin::mCherry (magenta) in an *unc-6* mutant animal. UNC-40::GFP localizes to the site of basement membrane breach (arrows) in *unc-6* mutants to a similar extent as wild-type animals (2.21-fold enrichment at breach relative to the invasive cell membrane in *unc-6* mutants and 2.48-fold enrichment in wild-type animals; $n = 10$ animals examined for each; $P > 0.43$, Student's *t* test). (D) Graphs show the fold enrichment of MIG-2 and UNC-34 at the initial basement membrane breach (relative to the rest of the invasive membrane). The fold enrichment of MIG-2 and UNC-34 at the initial basement membrane breach was reduced in *unc-40 (e271)* (MIG-2 = 1.07-fold; UNC-34 = 0.97-fold) compared with wild type (MIG-2 = 1.74-fold; UNC-34 = 1.93-fold; $n \geq 10$ animals each marker/genotype; $P < 0.001$, Student's *t* test). The error bars represent the SEM.

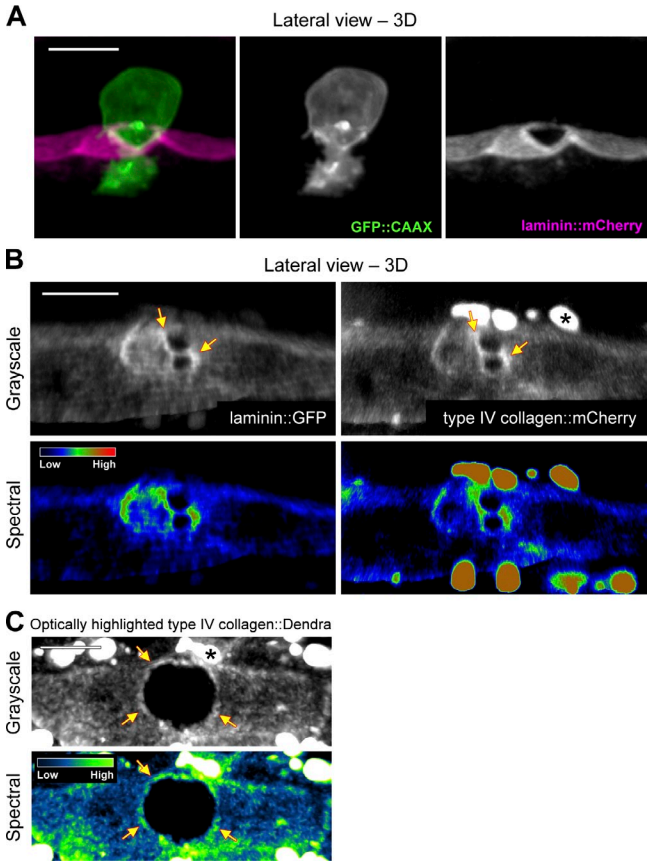

Figure S5. **The basement membrane is physically displaced during invasion.** (A) Images show how the invasive protrusion from the AC (visualized with GFP::CAAX membrane marker; green in overlay) maintains continuous contact with the edges of the expanding basement membrane gap (magenta). (B) Images of an animal coexpressing laminin::GFP (left) and type IV collagen::mCherry (right) show that both basement membrane components accumulate at the edge of the expanding basement membrane gap (arrows; grayscale above and spectral representation of fluorescence intensity below). Asterisks in B and C mark large intracellular accumulations of type IV collagen in neighboring muscle cells. (C) Images show accumulation of displaced optically highlighted type IV collagen::Dendra at the edges of the expanding basement membrane gap (arrows; grayscale above and spectral representation of fluorescence intensity below; see Fig. 6 B for experimental details). Bars, 5 µm.

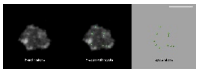

Video 1. **AC-invadopodia turn over dynamically before basement membrane breaching.** Ventral view time-lapse shows dynamic F-actin–rich AC-invadopodia (visualized with the F-actin probe *cdh-3* > mCherry::moeABD; left) prior to invasion. Images were acquired using a spinning disc confocal microscope (CSU-10 scan head; Yokogawa) mounted on a microscope (AxioImager; Carl Zeiss). Spot tracking analysis was performed in IMARIS 7.4 (Bitplane, Inc.) to quantify invadopodia dynamics (reported in Figs. S1 E and S3 C). A 60-min time-lapse is shown with time points acquired every 15 s. A projection of eight confocal z-sections (step size of 0.5 µm) is shown. The video plays at 10 frames per second. Bar, 5 µm. This video corresponds to the animal shown in Fig. 1 B.

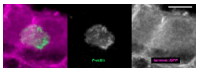

Video 2. **An AC-invadopodium presages and then occupies the site of basement membrane breach.** Ventral view time-lapse shows an AC-invadopodium (visualized with *cdh-3* > mCherry::moeABD in green) that presages (center, arrowhead) and then occupies the basement membrane breach (right, arrowhead). Images were acquired using a spinning disc confocal microscope (CSU-10 scan head; Yokogawa) mounted on a microscope (AxioImager; Carl Zeiss). A 30-min time-lapse is shown with time points acquired every 15 s. A projection of eight confocal z-sections (step size of 0.5 µm) is shown. Bar, 5 µm. This video corresponds to the animal shown in Fig. 1 E.

Video 3. **Invasive protrusion growth during basement membrane transmigration.** An AC is shown just after breaching the basement membrane (3D lateral view rotated forward). The video shows the AC's invasive protrusion (cyan) expanding through the basement membrane breach (magenta) and into the vulval tissue. The AC's cell membrane is visualized with a PI(4,5)P2 probe (*cdh-3* > mCherry::PLCδ^{PH}) and the basement membrane with laminin::GFP. Images were acquired using a spinning disc confocal microscope (CSU-10 scan head; Yokogawa) mounted on a microscope (AxioImager; Carl Zeiss). A 60-min time-lapse is shown with time points acquired every minute. A projection of seven confocal z-sections (step size of 1 µm) is shown. Bar, 5 µm. This video corresponds to the animal shown in Fig. 2 A.

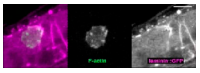

Video 4. **The invadopodia-to-invasive protrusion transition.** Ventral view time-lapse shows the transition between dynamic AC-invadopodia (visualized with the F-actin probe *cdh-3* > mCherry::moeABD in green) and the formation of a stable protrusion at the site of basement membrane breaching (visualized with laminin::GFP in magenta). Halfway through the video, AC-invadopodia cease to form along the remainder of the AC–basement membrane interface (overlay on left), as an invasive protrusion expands rapidly through the basement membrane and the corresponding breach widens radially. Images were acquired using a spinning disc confocal microscope (CSU-10 scan head; Yokogawa) mounted on a microscope (AxioImager; Carl Zeiss). A 60-min time-lapse is shown with time points acquired every 15 s. A projection of eight confocal z-sections (step size of 0.5 µm) is shown. Video is played at 20 frames per second. Bar, 5 µm.

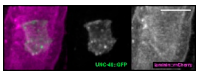

Video 5. **UNC-40::GFP enriches at the basement membrane breach.** Ventral view time-lapse shows UNC-40::GFP (green) enriching at the site of basement membrane breach (visualized with laminin::mCherry in magenta). Images were acquired using a spinning disc confocal microscope (CSU-10 scan head; Yokogawa) mounted on a microscope (AxioImager; Carl Zeiss). A 60-min time-lapse is shown with time points acquired every 2 min. A projection of eight confocal z-sections (step size of 0.5 µm) is shown. Bar, 5 µm. This video corresponds to the animal shown in Fig. 3 B.

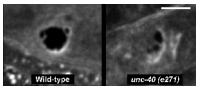

Video 6. **UNC-40 accelerates basement membrane gap opening.** Ventral view time-lapses show similarly sized basement membrane gaps (visualized with laminin::GFP) in a wild-type and an *unc-40* mutant animal. The basement membrane breach in the *unc-40* mutant animal opens at half the rate of the wild-type animals (for quantification see Fig. 4 F). Images were acquired using a spinning disc confocal microscope (CSU-10 scan head; Yokogawa) mounted on a microscope (AxioImager; Carl Zeiss). A 60-min time-lapse is shown with time points acquired every 2 min. A projection of eight confocal z-sections (step size of 0.5 µm) is shown. Bar, 5 µm. This video corresponds to the animals shown in Fig. 4 E.

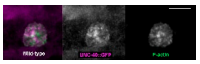

Video 7. **F-actin formation is focused at sites of UNC-40::GFP enrichment.** Ventral view time-lapse reveals recurrent F-actin formation (visualized with *cdh-3* > mCherry::moeABD in green) at the site-stable UNC-40::GFP (magenta) enrichment. Images were acquired using a spinning disc confocal microscope (CSU-10 scan head; Yokogawa) mounted on a microscope (AxioImager; Carl Zeiss)). A 60-min time-lapse is shown with time points acquired every 15 s. A projection of eight confocal z-sections (step size of 0.5 µm) is shown. Bar, 5 µm. This video corresponds to the animal and time-lapse summation shown in Fig. 5 B.

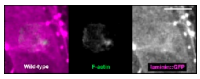

Video 8. **F-actin formation is focused at the basement membrane breach in wild-type animals.** Ventral view time-lapse shows recurrent F-actin formation (visualized with *cdh-3* > mCherry::moeABD in green) at the site of basement membrane breach (visualized with laminin::GFP in magenta) in a wild-type animal. Images were acquired using a spinning disc confocal microscope (CSU-10 scan head; Yokogawa) mounted on a microscope (AxioImager; Carl Zeiss)). A 60-min time-lapse is shown with time points acquired every 15 s. A projection of eight confocal z-sections (step size of 0.5 µm) is shown. Bar, 5 µm. This video corresponds to the wild-type animal and time-lapse summation shown in Fig. 5 C.

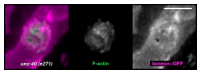

Video 9. **F-actin formation is not focused at basement membrane breaches in *unc-40* mutants.** Ventral view time-lapse demonstrates that dynamic F-actin formation (visualized with *cdh-3* > mCherry::moeABD in green) is not tightly correlated with the sites of basement membrane breach (visualized with laminin::GFP in magenta) in an *unc-40 (e271)* mutant animal. Images were acquired using a spinning disc confocal microscope (CSU-10 scan head; Yokogawa) mounted on a microscope (AxioImager; Carl Zeiss). A 60-min time-lapse is shown with time points acquired every 15 s. A projection of eight confocal z-sections (step size of 0.5 µm) is shown. Bar, 5 µm. This video corresponds to the *unc-40 (e271)* animal and time-lapse summation shown in Fig. 5 C.

Table S1. **Primer sequences and templates used for all PCR fusions generated**

Primer sequence	Primer type	Amplicon	Template
5′-TAATgTgAgTTAgCTCACTCATTAgg-3′	forward	*cdh-3* > promoter	pPD107.94/mk62-63
5′-AACgATggATACgCTAACAACTTgg-3′	forward nested	*cdh-3* > promoter	pPD107.94/mk62-63
5′-TTTCTgAgCTCggTACCCTCCAAg-3′	reverse	*cdh-3* > promoter	pPD107.94/mk62-63
5′-ATgAgTAAAggAgAAgAACTTTTC-3′	forward	*GFP*	pPD95_81
5′-TTTgTATAgTTCATCCATgCCATg-3′	reverse	*GFP*	pPD95_81
5′-CTTggAgggTACCgAgCTCAgAAAATggATACgCTAACAACTTgg-3′	*cdh-3* extension, forward	*Lifeact::GFP*	pJWZ73
5′-TTTCACCAgCgTTTCTgggTgAgC-3′	reverse	*Lifeact::GFP*	pJWZ73
5′-TggTgCACTCTCAgTACAATCTgC-3′	reverse nested	*Lifeact::GFP*	pJWZ73
5′ ACtATAgggCgAATTgggTACCgg-3′	forward	*GFP::PLCδ^{PH}*	*pBsSK-GFP-PLCδ^{PH}*
5′-CTTggAgggTACCgAgCTCAgAAAATggTCTCAAAgggTgAAgAAgAT-3′	*cdh-3* extension, forward nested	*GFP::PLCδ^{PH}*	*pBsSK-GFP-PLCδ^{PH}*
5′-TTACTTCTgCCgCTggTCCATggA-3′	reverse	*GFP::PLCδ^{PH}*	*pBsSK-GFP-PLCδ^{PH}*
5′-ATTACACATggCATggATgAACTAATgTCTTCACCgTCgAggCAgATC-3′	*gfp* extension, forward	*MIG-2*	N2 genomic DNA
5′-AAAAACgACTCAATAggTgAgCgC-3′	reverse	*MIG-2*	N2 genomic DNA
5′-gTTgCTCTAAAAACCCgATCTTCC-3′	reverse nested	*MIG-2*	N2 genomic DNA
5′-ATTACACATggCATggATgAACTAATgCAAgCgATCAAATgTgTCgTC-3′	*gfp* extension, forward	*CED-10*	N2 genomic DNA
5′-TTCTATCAAATggAAgCACAgCgg-3′	reverse	*CED-10*	N2 genomic DNA
5′-TTgATTAgAACTTTTgAATTTCCC-3′	reverse nested	*CED-10*	N2 genomic DNA
5′-CTTggAgggTACCgAgCTCAgAAAATgAgTAAAggAgAAgAACTTTTC-3′	*cdh-3* extension, forward	*GFP::CAAX*	pSA129
5′-TATCAgggTTATTgTCTCATgAgC-3′	reverse	*GFP::CAAX*	pSA129
5′-AgCgAggACAATTCTCATCgTTCg-3′	reverse nested	*GFP::CAAX*	pSA129
5′-TCCATggACCAgCggCAgAAgTAACAACTgAgCgCCggTCgCTACCAT-3′	*PLCδ^{PH}* extension, forward	*unc-54* 3′UTR	pPD95_81
5′-TTTCACCAgCgTTTCTgggTgAgC-3′	reverse	*unc-54* 3′UTR	pPD95_81
5′-gTgCCACCTgACgTCTAAgAAACC-3′	reverse nested	*unc-54* 3′UTR	pPD95_81
5′-TggTgCACTCTCAgTACAATCTgC-3′	reverse nested 2	*unc-54* 3′UTR	pPD95_81

Table S2. **Extrachromosomal arrays and integrated stains generated**

Ex designation	Is designation	PCR fusion created	Injected concentration	Coinjection marker
qyEx234	*qyIs242*	*cdh-3 > Lifeact::GFP*[a]	0.2 ng/ml	unc-119+
qyEx231	*qyIs219*	*cdh-3 > GFP::PLCδ^{PH}* [a,b]	0.01 ng/ml	unc-119+
qyEx232	*qyIs220*	*cdh-3 > GFP::MIG-2*[c,d]	0.2 ng/ml	unc-119+
qyEx233	*qyIs221*	*cdh-3 > GFP::CED-10*[c,d]	0.1 ng/ml	unc-119+
qyEx191	*qyIs166*	*cdh-3 > GFP::CAAX*[a]	0.1 ng/ml	unc-119+

[a]3′UTR from the *unc-54* gene was included at the 3′ end of the construct.
[b]Construct was built using a three-step PCR fusion.
[c]The endogenous 3′ UTR was used.
[d]Coding regions were linked to a *cdh-3 > GFP* amplicon in the last step of the PCR fusion.